Amplitude-preserved wave-equation migration

Paul Sava and Biondo Biondi[1]

ABSTRACT

We analyze the amplitude variation as a function of reflection angle (AVA) for angle-domain common image gathers (ADCIG) produced via wave-equation migration. Straightforward implementations of the two main ADCIG methods lead to contradictory, thus inaccurate, amplitude responses. The amplitude inaccuracy is related to the fact that downward-continuation migration is the adjoint of upward-continuation modeling, but it is only a poor approximation of its inverse. We derive the frequency-wavenumber domain diagonal weighting operators that make migration a good approximation to the inverse of modeling. With these weights, both ADCIG methods produce consistent results. The main applications that follow from this paper are true-amplitude migration and pseudo-unitary modeling/migration, usable for iterative inversion. The two most important factors that degrade the accuracy of wave-equation ADCIGs are the limited sampling and offset range, combined with the band-limited nature of seismic data.

INTRODUCTION

Traditionally, migration velocity analysis and AVO employ offset-domain common-image gathers, since most of the relevant information is not described by zero-offset or stacked images. However, it is difficult to produce these gathers with wave-equation migration because the offset dimension of the downward continued data shrinks with depth. A solution to this problem is to use angle-gathers instead of offset-gathers. Angle-domain common image gathers (ADCIG) obtained by wave-equation migration are very powerful at measuring the quality of migration and the accuracy of the velocity model.

ADCIGs are attractive because they provide straightforward information for amplitude analysis, that is, amplitude versus angle (AVA) instead of the more common amplitude versus offset (AVO) analysis. The main focus of this paper is to evaluate how accurate is the the amplitude response of wave-equation migration as a function of reflection angle.

Angle-domain common-image gathers are representations of the seismic images sorted by the incidence angle at the reflection point. Angle-gathers can be obtained using wave-equation techniques either for shot-profile migration, as described by de Bruin et al. (1990), or for shot-geophone migration, as described by Prucha et al. (1999). In either case, angle-gathers are evaluated using slant-stacks on the downward continued wavefield, prior to imaging. However,

[1]**email:** paul@sep.stanford.edu, biondo@sep.stanford.edu

decomposing the downward continued wavefield before imaging produces angle-gathers as a function of the less intuitive offset ray-parameter instead of the true reflection angle. Angle-domain gathers can also be computed by slant-stacking the image, instead of the downward continued wavefield. This alternative procedure directly produces angle-gathers as a function of reflection angle. In both cases, the slant-stack transformation can be more conveniently performed by a radial-trace transform (RTT) in the frequency-wavenumber domain (Ottolini, 1982).

AVA analysis requires that the procedures used to compute ADCIGs preserve the amplitude of the reflections as a function of angle. It is thus puzzling that straightforward implementations of both ADCIG methods produce contradictory amplitudes, and that downward-continuation migration is not a good approximation of the corresponding upward-continuation modeling for either method.

To solve the puzzle, we must take into account the weighting function that is introduced in the migration process by the imaging step. We show that this weighting is well approximated by a diagonal operator in the frequency-wavenumber domain. Since the two methods for computing ADCIGs perform a slant-stack at different stages, one before imaging and the other one after imaging, the corresponding weighting functions are different. Once the weights are taken into account, the AVA responses produced by the two methods are consistent, and migration is an approximate inverse of forward modeling. We find that, when restricted to flat reflectors, the weight we obtain for amplitude compensation is identical to those derived by Wapenaar et al. (1999).

According to the physical model for reflection data, the weights can be set to make migration a good approximation of a linearized inversion. We adopt the physical model proposed by Stolt and Benson (1986) and define the appropriate weights for both methods used to compute ADCIGs. Modeling and migration can also be easily made pseudo-unitary, if needed for an iterative estimation procedure. We achieve this by splitting in half the weighting factor between modeling and migration.

MODELING AND MIGRATION AMPLITUDES

This section sets the general framework of amplitude analysis and correction in relation to wave-equation modeling and migration.

The data (D) recorded at the surface can be modeled from the image (I) by integrating over depth (z) all the contributions of the reflected wavefield

$$D(\omega) = \int_0^{+\infty} dz\, e^{ik_z z} I(z), \tag{1}$$

where the vertical wavenumber (k_z), given by the double square root (DSR) equation, is the sum of two components: k_{zs} for continuing the sources, and k_{zr} for continuing the receivers ($k_z = k_{zs} + k_{zr}$). The expressions for k_{zs} and k_{zr} depend on the migration type and CIG type. However, the discussion in this section is general and independent of the particular expressions for k_{zs} and k_{zr}.

The image is linked to physical parameters, such as reflectivity (R), by a reflection operator (G) that relates the upgoing wavefield, to the downgoing wavefield, such that $I = GR$. The form of this reflection, or scattering, operator depends on the physical model adopted for the reflection process.

In the case of constant velocity, for which we can use the definitions introduced by Clayton and Stolt (1981) and Stolt and Benson (1986), the operator (G) is a simple frequency-wavenumber domain multiplication defined by

$$G = \frac{i\omega s^2}{4k_{zs}k_{zr}}. \tag{2}$$

Amplitude correction in constant velocity

Migration is, by the standard definition, the operation adjoint to forward modeling. It is performed by the downward continuing the recorded wavefield and imaging at zero time:

$$\widehat{I(z)} = \int_{-\infty}^{+\infty} d\omega\, e^{-ik_z z} D(\omega). \tag{3}$$

We substitute Equation (1) into Equation (3), and expand the integral in Equation (1) to negative depth, for which the image is zero, by definition:

$$\widehat{I(z)} = \int_{-\infty}^{+\infty} d\omega\, e^{-ik_z z} \int_{-\infty}^{+\infty} dz'\, e^{ik_z z} I\left(z'\right). \tag{4}$$

We then change the integration variable ω to k_z and obtain:

$$\widehat{I(z)} = \int_{-\infty}^{+\infty} dk_z\, e^{-ik_z z} \frac{d\omega}{dk_z} \int_{-\infty}^{+\infty} dz'\, e^{ik_z z} I\left(z'\right). \tag{5}$$

The pair of integrals in Equation (5) describe forward and inverse Fourier transforms, and thus the effect of chaining modeling and migration on the image is simply the equivalent of applying the Jacobian $d\omega/dk_z$. This result is valid only for real values of k_z, which is what we want, since we are not interested in the wavefield component for which k_z becomes imaginary (that is, we neglect evanescent waves).

In constant velocity, the frequency-wavenumber representation of the Jacobian is simply a multiplication:

$$\begin{aligned} \widehat{I(k_z)} &= \frac{d\omega}{dk_z} I(k_z) \\ &= \frac{d\omega}{dk_z} G(k_z) R(k_z). \end{aligned} \tag{6}$$

The Jacobian weighting is introduced by the imaging step, therefore, the Jacobian depends on the coordinates used to define the wavefield during imaging: constant ray-parameter or constant offset wavenumber.

In matrix notation, Equation (1) is written

$$\mathbf{d} = \mathbf{L}\mathbf{i} = \mathbf{L}\mathbf{G}\mathbf{r}, \tag{7}$$

where **d**, **i**, and **r** are respectively the data, image, and reflectivity vectors, **G** is a diagonal matrix representing the reflection operator, and **L** is the modeling operator. With this notation, Equation (5) becomes

$$\widehat{\mathbf{i}} = \mathbf{L}^*\mathbf{d} = \mathbf{L}^*\mathbf{L}\mathbf{i} = \mathbf{W}\mathbf{i} = \mathbf{W}\mathbf{G}\mathbf{r}, \tag{8}$$

where **W** is a diagonal matrix representing the Jacobian $d\omega/dk_z$.

Amplitude correction in variable velocity

The results presented in the preceding subsection are strictly valid in constant velocity. When velocity varies, the propagation operator (**L**) is not only a constant magnitude phase-shift multiplication, but also includes an amplitude term that changes with depth and horizontal location. Therefore, the integrals in Equation (5) cannot be interpreted as Fourier transforms anymore. Clayton and Stolt (1981) show how this issue can be theoretically side-stepped by datuming the data just above each reflector, and by approximating the velocity as constant in the imaging interval. In practice, this issue is taken care of by evaluating the Jacobian and the reflection operator G, using the local velocity at the imaging location.

When the continuation equation includes the amplitude term (**A**), Equation (7) becomes

$$\mathbf{d} = \mathbf{L}\mathbf{A}\mathbf{i} = \mathbf{L}\mathbf{A}\mathbf{G}\mathbf{r}. \tag{9}$$

Since conventional migration is the adjoint of modeling, Equation (8) becomes

$$\widehat{\mathbf{i}} = \mathbf{A}^*\mathbf{L}^*\mathbf{d} = \mathbf{A}^*\mathbf{L}^*\mathbf{L}\mathbf{A}\mathbf{i} = \mathbf{A}^*\mathbf{W}\mathbf{A}\mathbf{i} = \mathbf{A}^*\mathbf{W}\mathbf{A}\mathbf{G}\mathbf{r}, \tag{10}$$

In layered media, the frequency-wavenumber amplitude term of the continuation operator can be computed using the WKBJ approximation as a diagonal real operator (Clayton and Stolt, 1981):

$$A = \sqrt{\frac{k_{zs}(z)}{k_{zs}(z=0)}\frac{k_{zr}(z)}{k_{zr}(z=0)}}, \tag{11}$$

where k_{zs} and k_{zr} are the depth wavenumbers associated with source and receiver.

APPLICATIONS OF AMPLITUDE-PRESERVED MIGRATION

Two important applications derive from the theoretical development of amplitude-preserving migration: “true-amplitude” migration operators, and pseudo-unitary modeling/migration operators used in iterative inversion.

True-amplitude migration

We define "true-amplitude" migration as the process of recovering the amplitude of the reflectivity vector given perfect data, infinite bandwidth and aperture.

The expression for the true-amplitude migration operator is

$$\mathbf{L}_t^* = \mathbf{G}^{-1}\mathbf{A}^{-1}\mathbf{W}^{-1}\mathbf{L}^*, \tag{12}$$

which we can immediate verify to be inverse to modeling using Equation (9):

$$\mathbf{L}_t^*\mathbf{d} = \mathbf{G}^{-1}\mathbf{A}^{-1}\mathbf{W}^{-1}\mathbf{L}^*\mathbf{LAGr} = \mathbf{r}. \tag{13}$$

Even in the simple case of layered media, the operator $\mathbf{A}$ is singular for evanescent waves propagating at the surface, and null, thus not invertible, for evanescent waves at depth. As discussed in the preceding section, we are not interested in the evanescent energy, and thus we are not even trying to invert $\mathbf{A}$ for those wavefield components.

Pseudo-unitary modeling/migration

The "true-amplitude" migration defined in Equation (12) is a good approximation in the case of mild velocity variations, commonly labeled as "time-migration" problems. In complex overburden, the so called "depth-migration" situations, the reflectors are sparsely and unevenly illuminated (Rickett, 2001), therefore the amplitude corrections described in the preceding sections may become a poor approximation. In these cases, the amplitude term ($\mathbf{A}$) is neither diagonal nor invertible because of reflections becoming evanescent and/or moving out of the acquisition aperture. Direct inversions are not likely to produce good results, therefore we have to solve the inversion problem using iterative schemes (Prucha et al., 2001). Thus, instead of simply applying "true-amplitude" migration, we iteratively solve the least-squares problem described by the optimization goal

$$(\mathbf{LAG})\,\mathbf{r} \approx \mathbf{d} \tag{14}$$

where the operator $\mathbf{LAG}$ fits the reflectivity model ($\mathbf{r}$) to the recorded data ($\mathbf{d}$).

In order to achieve fast convergence, the modeling operator has to be as close to unitary as possible. Following the discussion in the preceding sections, we can define the pseudo-unitary operator as

$$\mathbf{L}_u = \mathbf{L}\mathbf{W}^{-\frac{1}{2}} \tag{15}$$

for which it is immediate to verify that $\mathbf{L}_u^*\mathbf{L}_u = \mathbf{I}$.

With this new operator, our least-squares problem may be rewritten as:

$$\left(\mathbf{L}_u\mathbf{W}^{\frac{1}{2}}\mathbf{AG}\right)\mathbf{r} \approx \mathbf{d}.$$

We can redefine the model variable as a new, preconditioned variable

$$\mathbf{p} = \mathbf{W}^{\frac{1}{2}}\mathbf{AGr},$$

which changes the optimization problem to the simple equation:

$$\mathbf{L}_u\mathbf{p} \approx \mathbf{d}. \tag{16}$$

ADCIG METHODS

Angle-domain common-image gathers are the instrument we use to analyze the amplitude variation with reflection angle. As we discussed in in an earlier section, ADCIGs can be conveniently formed in the frequency domain. Following the derivation of Fomel (1996), if

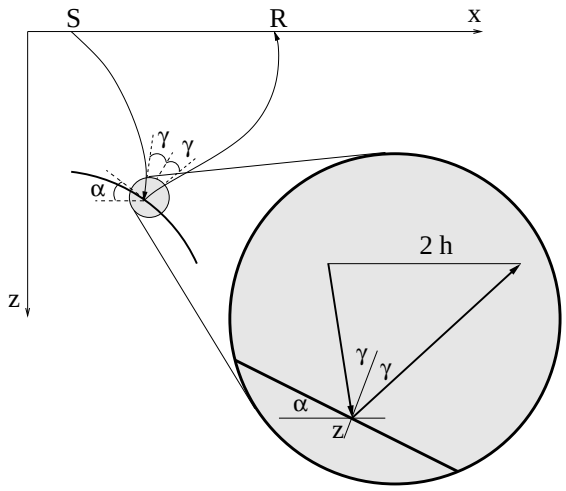

Figure 1: A scheme of reflection rays in an arbitrary-velocity medium. paul2-local [NR]

we consider that, in constant velocity media, t is the traveltime from the source to the reflector and back to the receiver at the surface, $2h$ is the offset between the source and the receiver, z is the depth of the reflection point, α is the geologic dip, γ is the reflection angle, and s is the slowness (Figure 1), we can write

$$p_h = \frac{\partial t}{\partial h} = 2s\cos\alpha\sin\gamma \tag{17}$$

$$-\frac{\partial t}{\partial z} = 2s\cos\alpha\cos\gamma. \tag{18}$$

Combining Equations (17) and (18), we find that

$$\tan\gamma = -\left.\frac{\partial z}{\partial h}\right|_{t,x}. \tag{19}$$

Equation (19) is derived in constant velocity media, but it remains perfectly valid in a differential sense in any arbitrary velocity media if we consider h to be the effective offset at the reflector depth and not the surface offset (Figure 1).

In the frequency-wavenumber domain (Sava and Fomel, 2000), formula (19) takes the trivial form

$$\tan\gamma = -\frac{k_h}{k_z}. \tag{20}$$

This equation indicates that angle-gathers can be conveniently formed with the help of frequency-domain migration algorithms (Stolt, 1978). Furthermore, wave-equation migration is ideally suited to compute angle-gathers using such a method, since the migration output is precisely described by the offset at the reflector depth, which is a model parameter, and not by the surface offset, which is a data parameter (Biondi, 1999).

We can also recognize that Equation (17) describes nothing but the ray parameter of the propagating wave at the incidence with the reflector. Using the definition

$$p_h = \frac{\partial t}{\partial h},$$

it follows that we can write a relation similar to Equation (20) to evaluate the offset ray parameter in the Fourier-domain:

$$p_h = \frac{k_h}{\omega}. \tag{21}$$

Both Equations (20) and (21) can be used to compute image gathers through radial trace transforms (RTT) in the Fourier domain. The major difference is that Equation (20) operates in the space of the migrated image, while Equation (21) operates in the data space.

The two methods are also different in three other ways:

1. The image-space method (20) is completely decoupled from migration, therefore conversion to reflection angle can be thought of as a post-processing after migration. Such post-processing is interesting because it allows conversion from the angle domain back to the offset domain without re-migration (Figure 2), which is, of course, not true for the data-space method (21), where the transformation is a function of the data frequency (ω).

2. From Equation (17), it follows that offset ray parameter (p_h) is also a function of the structural dip (α), which is not true for the reflection angle (γ) estimated in the image space. The angles we obtain using Equation (20) are geometrical measures, completely independent on the structural dip. For AVA purposes, it is also very convenient to have the amplitudes as a function of reflection angle and not offset or offset ray-parameter.

3. Both methods require accurate knowledge of the imaging velocity. The difference is that the data-space method is less sensitive to the location of velocity boundaries. However, conversion from p_h to reflection angle γ is also critically influenced by errors in the velocity maps.

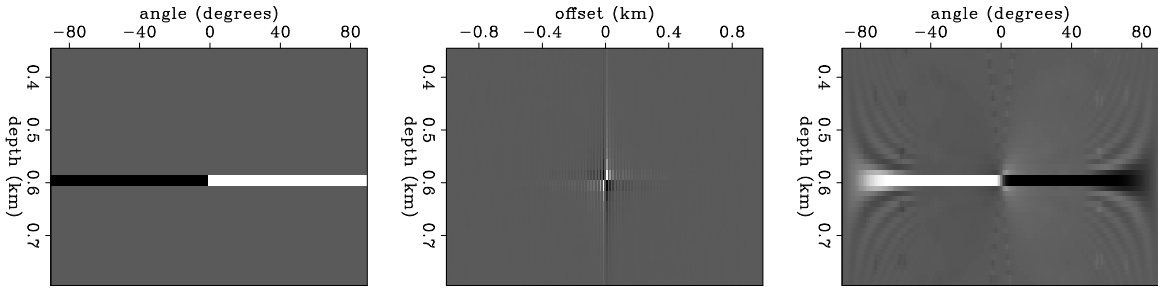

Figure 2: Synthetic example of conversion between the angle and offset domains in the image space. Left panel: synthetic angle gather. Middle panel: conversion from angle to offset. Right panel: conversion back to the angle domain. paul2-polarity [NR]

SOURCES OF INACCURACY

Figure 2 shows a synthetic example of conversion from the angle domain to offset domain and back to the angle domain. The original ADCIG is described by polarity reversal at zero incidence angle. After conversion to offset and back to angle, the image gather displays the same polarity reversal. The angle-gathers are also flat, which indicates that the transformation is kinematically correct.

The obvious question that remains to be addressed is how reliable in general are the amplitude versus angle estimates for images obtained using wave-equation migration.

As mentioned earlier, we compute the image-gathers either in the image space, or in the data space via Fourier-domain radial-trace transforms. Analysis of our procedure reveals four major sources of distorsion of the amplitude response which are: (1) the limited offset and depth wavenumber bandwidths, (2) the limited temporal frequency bandwidth, (3) the incorrect implementation of RTT, and (4) the unweighted imaging condition. In the next four subsections, we discuss each of these sources of error, and refer to image gathers in the angle domain, although the discussion is fully applicable to offset ray-parameter, as well.

We demonstrate the various transformations and sources of inaccuracy using a very simple synthetic model (Figure 3), which is a perfectly focused image (a spike in the offset domain).

Limited offset and depth wavenumber bandwidths

One of the main sources of amplitude error is the finite bandwidth of the depth (k_z) and offset (k_h) wavenumbers (Figure 4). We apply RTT in the Fourier domain using Equations (20). In practical terms, this transformation amounts to a horizontal stretch of k_h at constant k_z. However, since k_z and k_h are limited in range, we can correctly evaluate the angle transformation only within a finite angle range $(-\gamma_{max}, +\gamma_{max})$. The maximum angles to which our transformation is correct is a function of image sampling on offset and depth (Figure 4). γ_{max} can be evaluated from the data, but cannot be modified during processing. We simply need to be aware of it and limit our analysis to the proper angle range.

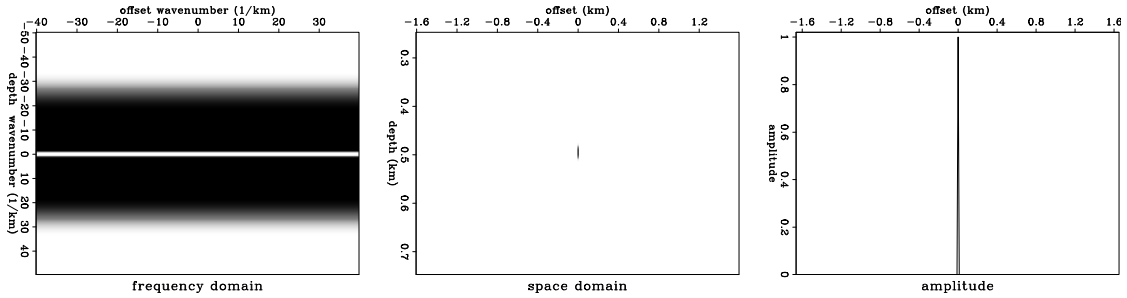

Figure 3: Synthetic offset-gather. From left to right, Fourier-domain representation, space-domain representation, and amplitude response. The image is represented by one single perfectly focused event at a depth of 0.5 km. paul2-offam [NR]

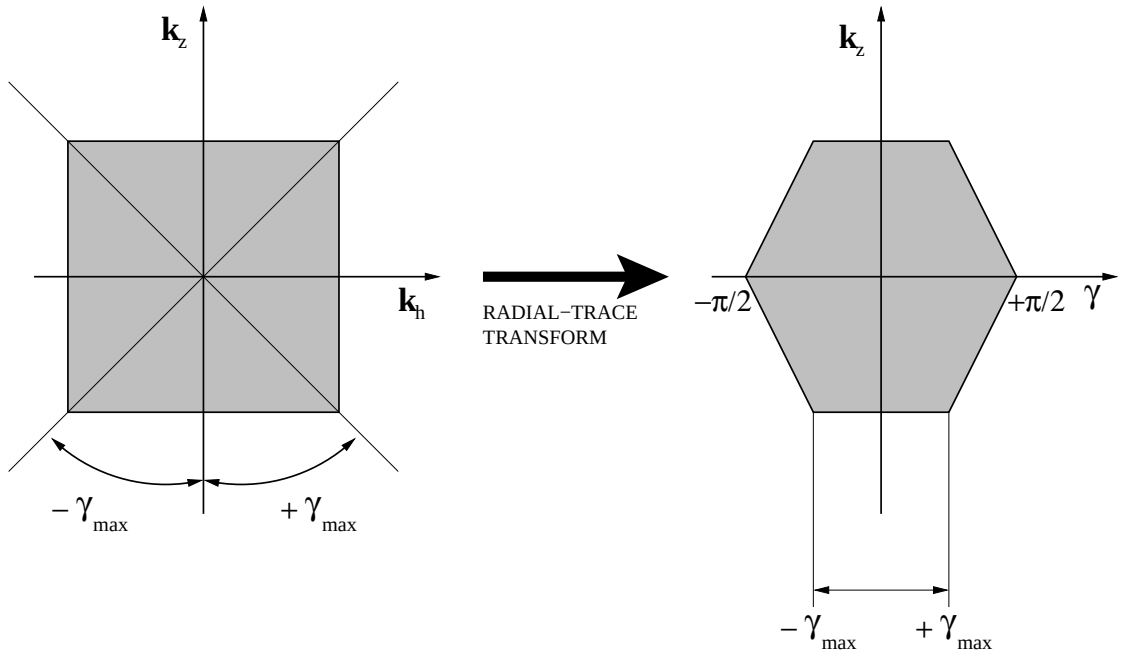

Figure 4: Truncation of the depth and offset wavenumber bandwidths limits the range over which we can compute angle-gathers. A $k_z - k_h$ offset-gather (left panel) is transformed by RTT to a $k_z - \gamma$ angle-gather (right panel). γ_{max} is the maximum angle for which the RTT is not affected by truncation of the k_h bandwidth. paul2-khband [NR]

Limited temporal frequency bandwidth

Another major source of inaccuracy is the limited temporal frequency band of the recorded data. Figure 5 schematically explains this phenomenon. We begin with an image gather in the offset domain, perfectly described in its limited $k_z - k_h$ band (a). From the image we model data described in $\omega - k_h$ coordinates (b). In the case of wide temporal frequency bands, we record the entire data (b, black shape). After migration, we return to the image domain (c, black shape) described by $k_z - k_h$ coordinates, from which we compute angle-gathers by RTT (d, black shape). Inverse Fourier transform along k_z brings us back in the angle domain, with correct amplitudes for all angles smaller than γ_{max}.

Alternatively, we can record a narrower frequency band (b, gray shape). After migration, we obtain the image as described by the DSR equation (c, gray shape). Conversion to angle follows the same style as in the full-band case (d, gray shape). The major distinction between the two cases is that we do not recover correct amplitudes even for the $(-\gamma_{max}, +\gamma_{max})$ range.

Again, this second cause of inaccuracy is related to data sampling and cannot be corrected during processing. One possible way to recover consistent amplitudes is to low-pass-filter the angle-domain gathers to appropriate maximum depth wavenumbers (k_z).

The same logic applies to offset ray-parameter gathers, as depicted in Figure 5 (e,f).

RTT implementation

A third source of inaccuracy is the actual implementation of the radial-trace transform. In theory, RTT can be implemented either as a push operator (loop over input) or as a pull operator (loop over output). Figure (6) shows an example with a push implementation (from the $k_z - k_h$ domain to the $k_z - \gamma$ domain), and Figure (7) shows a pull implementation (in the $k_z - \gamma$ domain from the $k_z - k_h$ domain).

As expected, the push implementation leaves empty regions in the $k_z - \gamma$ domain, while the pull implementation fills the entire domain. After inverse Fourier transform, the amplitude responses in the two cases are completely different (Figure 8): the pull implementation generates flat amplitudes, while the push implementation does not.

Under those circumstances, it would be tempting to consider just the pull implementation. However, inversion for angle-domain regularization, requires implementations for both the forward and adjoint operators. Therefore, if we use pull in one transformation, we need to use a corrected push in its adjoint (Claerbout, 1995). This correction is given by the Jacobian of the transformation from k_h to γ or p_h.

Figure 9 shows the angle-domain representation for the ideal offset-gather in Figure 3. Since we use a wide temporal frequency band and a pull implementation of RTT, the amplitude response is flat for the whole usable angle range.

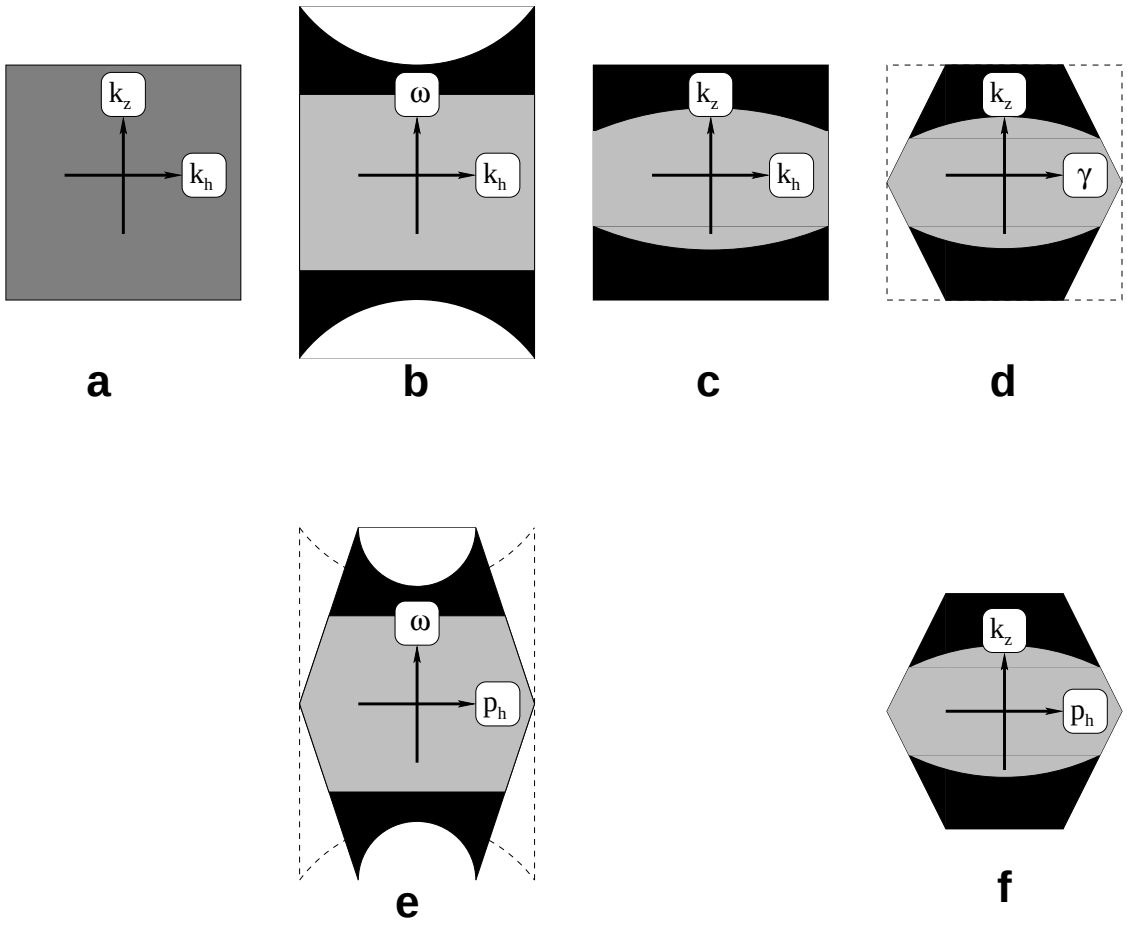

Figure 5: Schematic simulation of migration, modeling and conversion to the angle domain. For angle-domain gathers, start with the image in (a), model to obtain the data in (b), migrate (c), and convert to angle (d). For offset ray-parameter gathers, start with the image in (a), model to obtain the data in (b), convert to offset ray-parameter in the data space (e), and image (f). The black shapes correspond to a wide temporal frequency band, and the gray shapes correspond to band-limited data. paul2-adconv [NR]

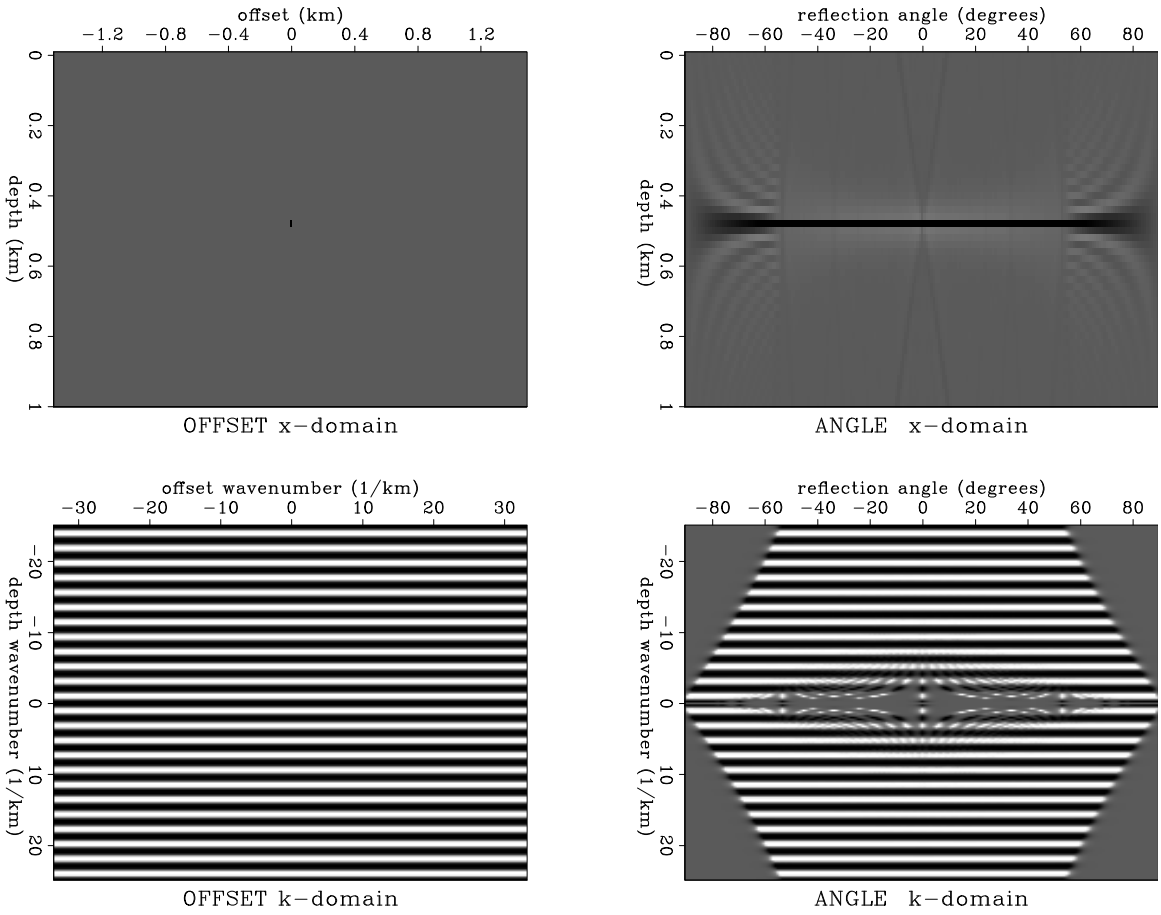

Figure 6: Conversion from offset-domain to angle-domain image gathers. The push implementation of RTT leaves empty spaces that degrade the amplitudes. This effect can be partially corrected by weighting with the transformation Jacobian. paul2-angpushA [NR]

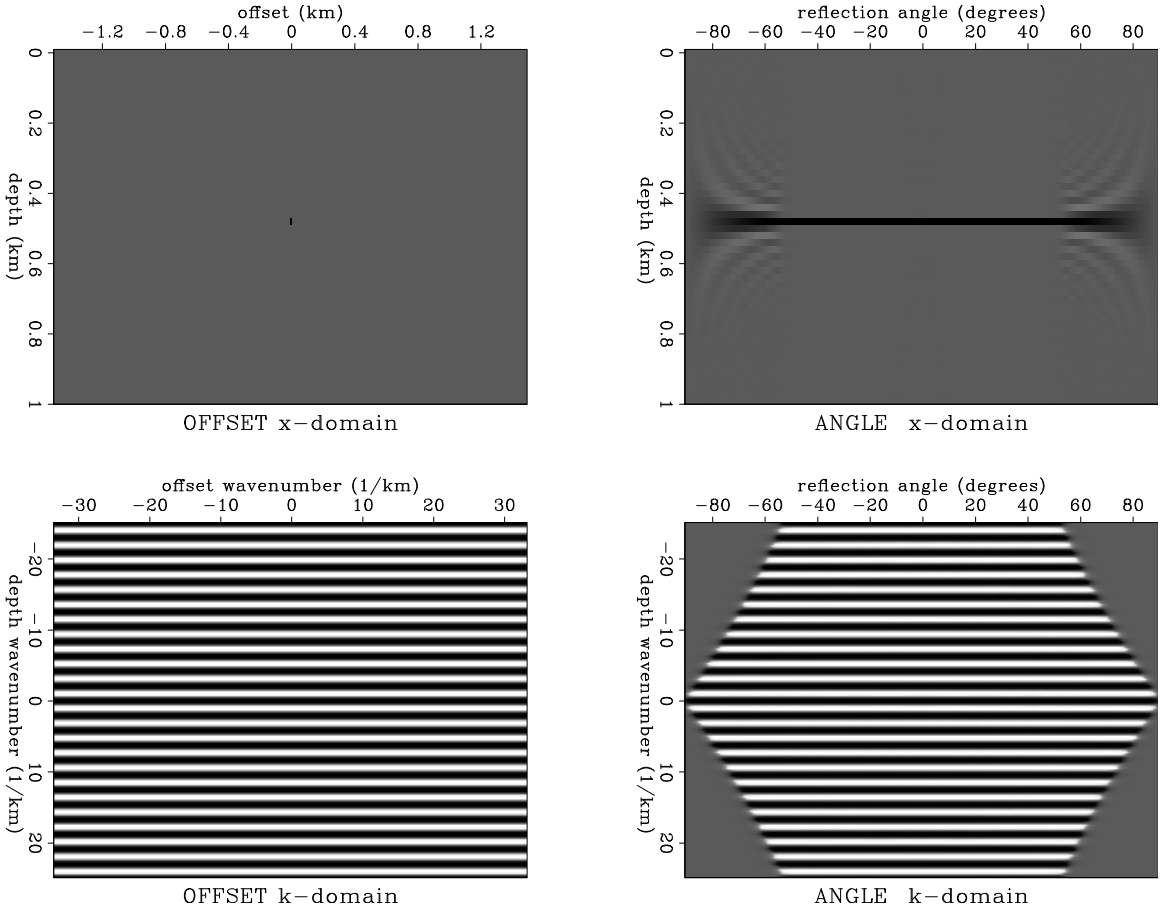

Figure 7: Conversion from offset-domain to angle-domain image gathers. The pull implementation of the RTT fills the entire usable space, therefore the amplitude response is correct. paul2-angpullA [NR]

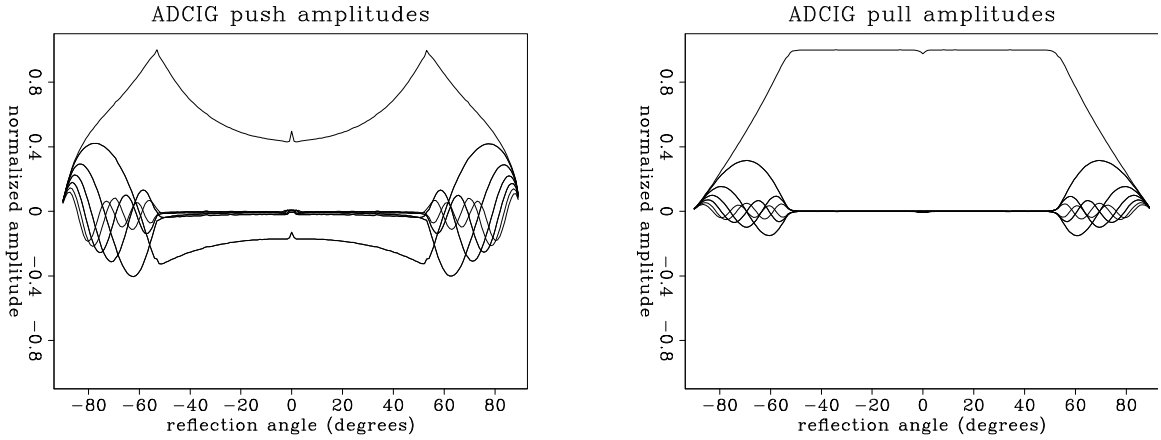

Figure 8: Amplitude response for RTT implemented as unweighted push (left), and pull (right). Ideally, the amplitude should be constant at all angles. paul2-ampA [NR]

Incorrect imaging condition

A more subtle source of error is related to the implementation of the modeling operator and its adjoint. In brief, conversion from the data space to the image space involves a change of coordinates from temporal frequency (ω) to depth wavenumber (k_z). A correct implementation of this transformation requires weighting by the transformation Jacobian. Figures 10 and 11 show the amplitude responses of modeling followed by migration without the Jacobian. Although the angle-gathers are kinematically correct (flat), the amplitude responses are not. More details on the Jacobian weighting follow in the next section.

TRANSFORMATION JACOBIANS

True-ampliude migration and the pseudo-unitary modeling/migration pair make use of the diagonal operator of the imaging Jacobian. In this section, we derive the analytical expression of this operator.

The two methods used to compute ADCIGs differ by the stage at which they operate: after imaging for ADCIGs with output in reflection-angle, and before imaging for ADCIGs with output in offset ray-parameter. Imaging takes place in different spaces as well: at constant k_h for reflection-angle image gathers, and at constant p_h for offset ray-parameter image gathers. Consequently, the imaging Jacobians have different expressions.

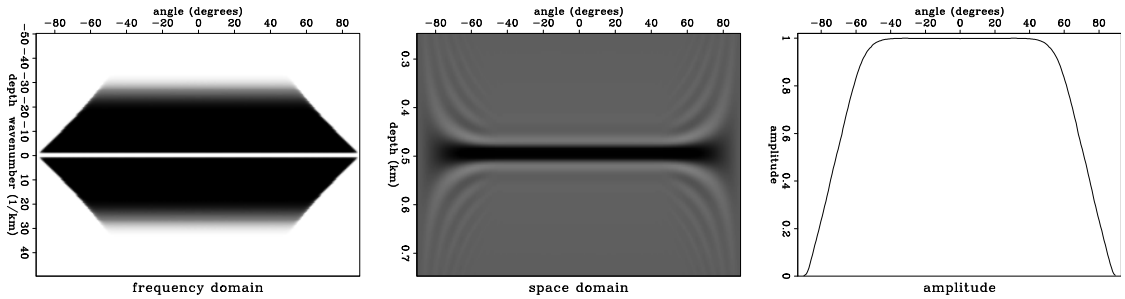

Figure 9: Ideal angle-gather for wide temporal frequency and pull implementation of RTT. From left to right, Fourier-domain, space-domain, and amplitude response. paul2-angam [NR]

Angle-gathers

For reflection-angle gathers, the dispersion relation used to downward continue the wavefield is given by the DSR equation:

$$\begin{aligned} k_z &= k_{zs} + k_{zr} \\ &= \frac{1}{2}\sqrt{(2\omega s)^2 - \left|\vec{k_m} - \vec{k_h}\right|^2} + \frac{1}{2}\sqrt{(2\omega s)^2 - \left|\vec{k_m} + \vec{k_h}\right|^2} \end{aligned} \tag{22}$$

where s is the local slowness, k_{zs} and k_{zr} are respectively the vertical wavenumber for the source and receiver components, and $\vec{k_m}$ and $\vec{k_h}$ are respectively the midpoint and offset wavenumbers. The Jacobian for this transformation is thus the common prestack Stolt migra-

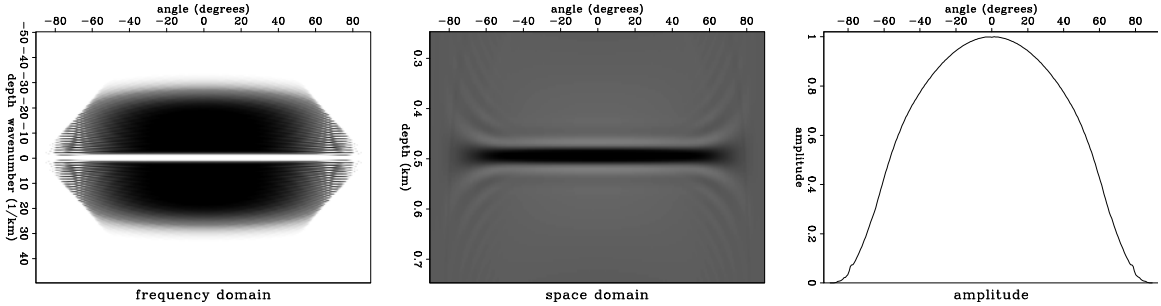

Figure 10: Reflection-angle gather implemented using Equation (20). We do not use the correct weighting of the transformation Jacobian, therefore the amplitudes are distorted. paul2-ghmig [NR]

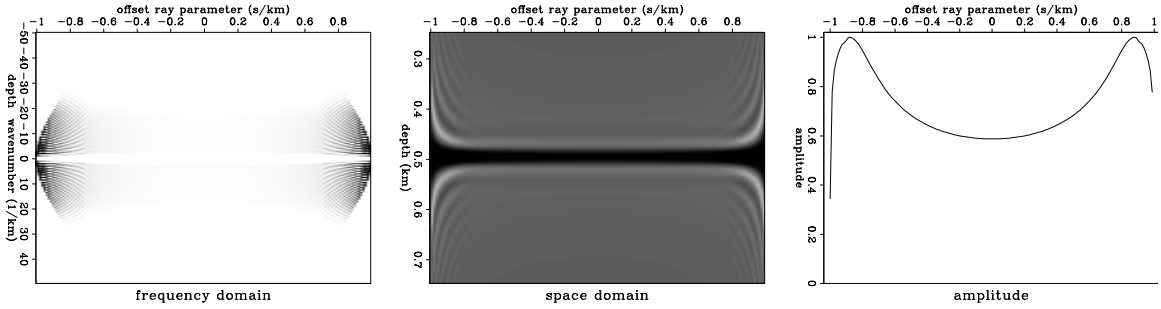

Figure 11: Offset ray-parameter gather implemented using Equation (21). We do not use the correct weighting of the transformation Jacobian, therefore the amplitudes are distorted. paul2-gpmig [NR]

tion Jacobian:

$$\begin{aligned} \mathbf{W}_{k_h} &= \left.\frac{d\omega}{dk_z}\right|_{\vec{k_h}=const} \\ &= \left[s\left(\frac{\omega s}{k_{zs}}+\frac{\omega s}{k_{zr}}\right)\right]^{-1}. \end{aligned} \tag{23}$$

As mentioned in the preceding sections, in the case of variable velocity media, those quantities are evaluated at the reflector location. For an arbitrary 2-D reflector geometry (Figure 1), we can rewrite Equation (23) as

$$\mathbf{W}_{k_h} = \left[s\left(\frac{1}{\cos\left[\gamma-\alpha\right]}+\frac{1}{\cos\left[\gamma+\alpha\right]}\right)\right]^{-1}, \tag{24}$$

where α is the structural dip angle, and γ is the reflection angle.

For flat reflectors, defined by $\vec{k_m} = 0$ and $\alpha = 0$, the Jacobian takes the simple form

$$\mathbf{W}_{k_h} = \frac{1}{2s}\cos\gamma. \tag{25}$$

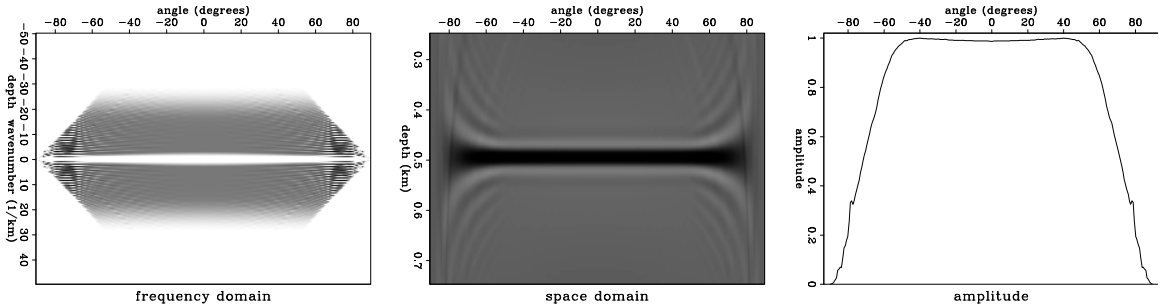

Figure 12: Reflection-angle gather computed in the image space. The weighting factors restore correct amplitudes. Compare with the theoretical response in Figure 10. paul2-chmig [NR]

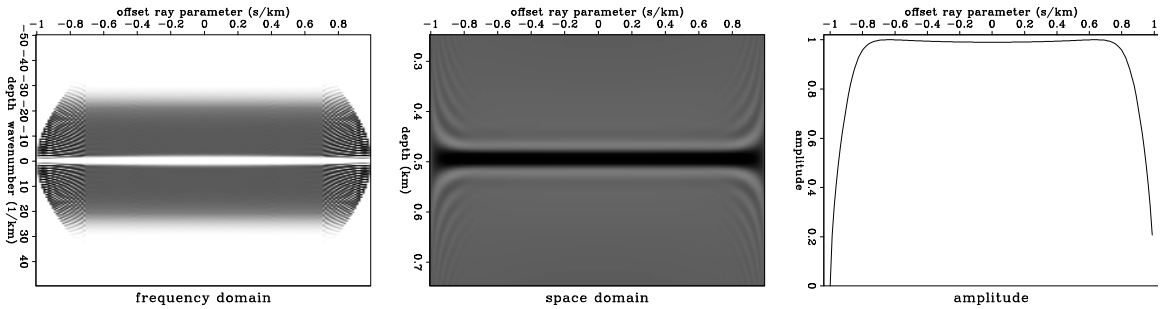

Figure 13: Offset ray-parameter gather computed in the data space. The weighting factors restore correct amplitudes. paul2-cpmig [NR]

Ray-parameter gathers

For the case of offset ray-parameter gathers, we can rewrite the DSR equation (22) as

$$\begin{aligned} k_z &= k_{zs} + k_{zr} \\ &= \frac{1}{2}\sqrt{(2\omega s)^2 - \left|\vec{k_m} - \omega\vec{p}_h\right|^2} + \frac{1}{2}\sqrt{(2\omega s)^2 - \left|\vec{k_m} + \omega\vec{p}_h\right|^2}. \end{aligned} \tag{26}$$

In this case, the imaging Jacobian becomes

$$\begin{aligned} \mathbf{W}_{p_h} &= \left.\frac{d\omega}{dk_z}\right|_{\vec{p}_h = const} \\ &= \left[\frac{4\omega s^2 + \left(\vec{k_m} - \omega\vec{p}_h\right)\cdot\vec{p}_h}{4k_{zs}} + \frac{4\omega s^2 - \left(\vec{k_m} + \omega\vec{p}_h\right)\cdot\vec{p}_h}{4k_{zr}}\right]^{-1}, \end{aligned} \tag{27}$$

which can be re-arranged as:

$$\mathbf{W}_{p_h} = \left[\left(s - \frac{\vec{p}_h \cdot \vec{p}_h}{4s}\right)\left(\frac{\omega s}{k_{\rm zs}} + \frac{\omega s}{k_{\rm zr}}\right) + \frac{\vec{k_m} \cdot \vec{p}_h}{4\omega s}\left(\frac{\omega s}{k_{\rm zs}} - \frac{\omega s}{k_{\rm zr}}\right)\right]^{-1}. \tag{28}$$

For an arbitrary 2-D reflection geometry (Figure 1), we can write Equation (28) as

$$\mathbf{W}_{p_h} = \left[\left(s - \frac{\vec{p}_h \cdot \vec{p}_h}{4s}\right)\left(\frac{1}{\cos\left[\gamma - \alpha\right]} + \frac{1}{\cos\left[\gamma + \alpha\right]}\right) + \frac{\vec{k_m} \cdot \vec{p}_h}{4\omega s}\left(\frac{1}{\cos\left[\gamma - \alpha\right]} - \frac{1}{\cos\left[\gamma + \alpha\right]}\right)\right]^{-1}. \tag{29}$$

For flat reflectors, defined by $\vec{k_m} = 0$ and $\alpha = 0$, the Jacobian takes the simple form

$$\mathbf{W}_{p_h} = \frac{1}{2s}\frac{1}{\cos\gamma}, \tag{30}$$

which is equivalent to the weighting factor introduced by Wapenaar et al. (1999).

For the case of flat reflectors, we also have

$$\mathbf{W}_{p_h} = \frac{1}{4s^2}\frac{1}{\mathbf{W}_{k_h}}. \tag{31}$$

which explains the opposite behavior of the *uncorrected* migration amplitudes for reflection-angle gathers (Figure 10) and offset ray-parameter gathers (Figure 11).

After we apply the Jacobian weights, we obtain the corrected angle-gathers shown in Figures 12 and 13. As expected, the amplitudes are constant for the entire usable angular range.

JACOBIAN FOR COMMON-AZIMUTH MIGRATION

The dispersion relation of 3-D common-azimuth migration can be written as a cascade of 2-D inline prestack migration and 2-D zero-offset crossline migration (Biondi, 1999):

$$\begin{aligned} k_{z_x} &= \frac{1}{2}\sqrt{(2\omega s)^2 - |k_{mx} - k_{hx}|^2} + \frac{1}{2}\sqrt{(2\omega s)^2 - |k_{mx} + k_{hx}|^2} \\ k_z^{\rm CA} &= \sqrt{k_{z_x}^2 - k_{my}^2}. \end{aligned} \tag{32}$$

We can derive the expression for the common-azimuth Jacobian by simply applying the chain rule to Equation (32):

$$\frac{dk_z^{\rm CA}}{d\omega} = \frac{dk_z^{\rm CA}}{dk_{z_x}}\frac{dk_{z_x}}{d\omega}. \tag{33}$$

If we note that

$$\frac{dk_z^{\rm CA}}{dk_{z_x}} = \frac{k_{z_x}}{k_z^{\rm CA}} \tag{34}$$

we obtain the common-azimuth Jacobian:

$$\mathbf{W}^{\text{CA}} = \frac{k_z^{\text{CA}}}{k_{z_x}} \mathbf{W}^{\text{2D}} \tag{35}$$

where $\mathbf{W}^{\text{2D}}$ is the 2-D version of the Jacobian we derived in the preceding sections, either for reflection-angle ADCIGs, Equation (23), or for offset ray-parameter, Equation (28).

However, computing the reflection operator weight, Equation (2), and the WKBJ amplitudes, Equation (11), requires us to evaluate separately the source k_{zs} and receiver k_{zr} components of the dispersion relation. Therefore, for the "true-amplitude" migration weights, Equation (12), we need to use the more complicated expression for the common-azimuth dispersion relation as introduced by Biondi and Palacharla (1996).

In addition to the amplitude terms we have discussed in the preceding sections, "true-amplitude" common-azimuth migration requires an additional correction that takes into account that its dispersion relation is obtained by a stationary-phase approximation of the full 3-D DSR equation. We, therefore, need to augment the amplitude term in Equation (9) by another factor, which results from stationary-phase approximation theory (Bleistein and Handelsman, 1975):

$$A_{\text{stat}} = \sqrt{\frac{2\pi}{\int_0^z \left| \frac{d^2 k_z^{\text{CA}}}{dk_{h_y}^2} \right| dz'}} e^{i \text{sgn}\left(\frac{d^2 k_z^{\text{CA}}}{dk_{h_y}^2} \right) \frac{\pi}{4}}, \tag{36}$$

where the second derivative of k_z^{CA} with respect to k_{h_y} is:

$$\begin{aligned} \frac{d^2 k_z^{\text{CA}}}{dk_{h_y}^2} = & - \frac{(2\omega s)^2 - (k_{m_x} - k_{h_x})^2}{\left[(2\omega s)^2 - (k_{m_x} - k_{h_x})^2 - \left(k_{m_y} - \widehat{k_{h_y}} \right)^2 \right]^{3/2}} \\ & - \frac{(2\omega s)^2 - (k_{m_x} + k_{h_x})^2}{\left[(2\omega s)^2 - (k_{m_x} + k_{h_x})^2 - \left(k_{m_y} + \widehat{k_{h_y}} \right)^2 \right]^{3/2}} \end{aligned} \tag{37}$$

with

$$\widehat{k_{h_y}} = k_{m_y} \frac{\frac{1}{2}\sqrt{(2\omega s)^2 - |k_{m_x} + k_{h_x}|^2} - \frac{1}{2}\sqrt{(2\omega s)^2 - |k_{m_x} - k_{h_x}|^2}}{\frac{1}{2}\sqrt{(2\omega s)^2 - |k_{m_x} + k_{h_x}|^2} + \frac{1}{2}\sqrt{(2\omega s)^2 - |k_{m_x} - k_{h_x}|^2}}. \tag{38}$$

This additional correction factor includes both a phase shift component and an amplitude component which increases with depth. It has thus a behavior similar to the correction term that is often used to transform 2-D data recorded with *point* sources and receivers to 2-D data recorded with *line* sources and receivers (Clayton and Stolt, 1981). The physical explanation is also analogous: Common-azimuth migration assumes that the data were recorded for all values of the crossline offset (h_y) and then stacked along h_y. The inverse of A_{stat} transforms the data recorded at zero crossline offset into the data "expected" by common-azimuth migration.

Figures 14-16 demonstrate the effects of applying the different weights in common-azimuth migration. These images are obtained by migrating a synthetic data set containing five dipping reflectors with dips from 0 to 60 degrees (Biondi, 2001).

Figure 14 shows a subset of the migration results. The front face of the cube displayed in the figure is an in-line section stacked over p_h. The other two faces are sections through the prestack image as a function of the offset ray parameter (p_h). Those images are obtained by migration without any weighting factors. Figure 15 shows the same subset as in Figure 14, but obtained by applying all the appropriate weights and the phase shift related to the stationary-phase approximation. The weights balance the amplitudes along the reflector, so that the dipping reflectors are comparable with the flat one.

Figure 16 shows one particular ADCIG, detailing the effects of each type of weighting: no weights (Figure 16a), Jacobian and modeling weights (Figure 16b), Jacobian, modeling and WKBJ weights (Figure 16c), and Jacobian, modeling, WKBJ and phase-shift weights (Figure 16d).

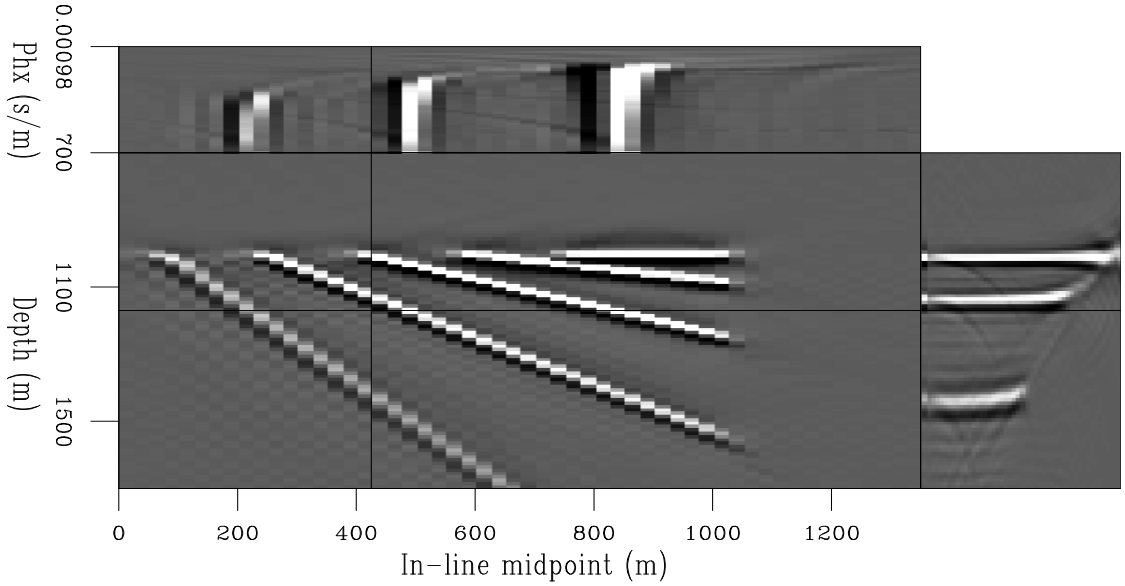

Figure 14: A subset of the results of common-azimuth migration of the synthetic data set. The front face of the cube is an in-line section stacked along p_h. The other two faces are sections through the prestack image. The migrated cube is obtained from migration without any weighting. The amplitudes of the dipping reflectors are lower than expected, and the whole image has the wrong phase. paul2-CA-pull-none-vp [NR]

VARIABLE-VELOCITY JACOBIANS

The transformation Jacobians, given by Equation (23) for reflection-angle gathers and by Equation (28) for offset ray-parameter gathers, are strictly speaking valid only for constant velocity media. In the case of variable velocity, downward continuation is implemented in the

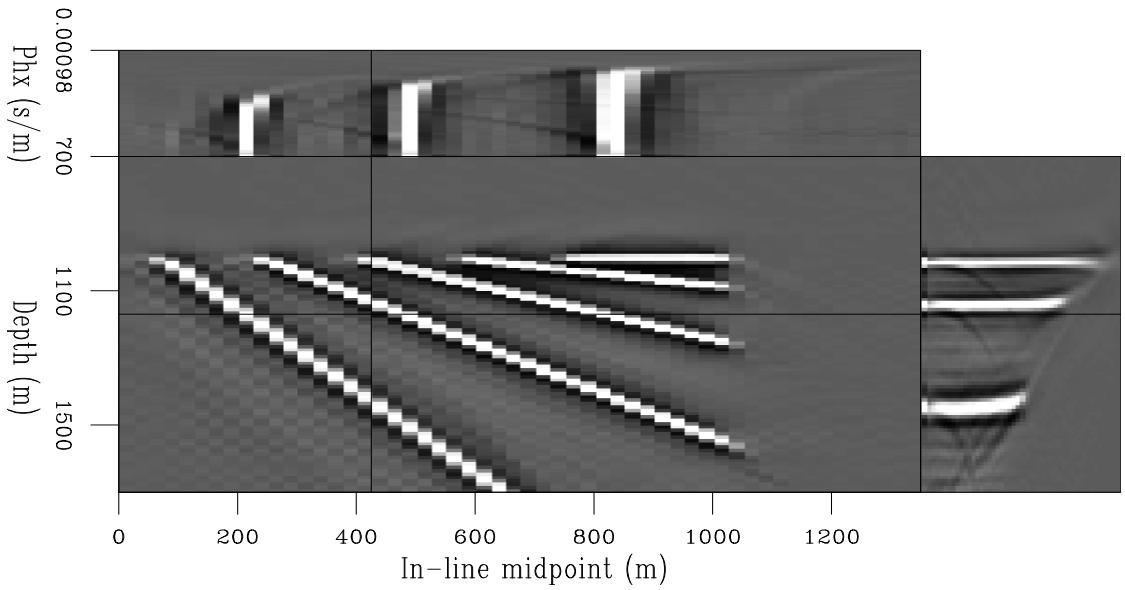

Figure 15: A subset of the results of common-azimuth migration of the synthetic data set. The front face of the cube is an in-line section stacked along p_h. The migrated cube is obtained from migration with all the appropriate weights and the stationary-phase phase shift. The amplitudes of the dipping reflectors are comparable with those of the flat reflector, and the whole image has the correct phase. paul2-CA-pull-WKBJ-stat-vp [NR]

mixt $\omega - k$ and $\omega - x$ domain. The dispersion relation is approximated using an expansion of the DSR equation. In one of the most usual forms, the dispersion relation can be written as

$$\begin{aligned} k_z &= k_{zs} + k_{zr} \\ k_{zs} &= \frac{1}{2}\sqrt{(2\omega s)^2 - \left|\vec{k}_s\right|^2} \approx k_{z0} + \left.\frac{dk_z}{ds}\right|_{s=so} (s_s - s_0) \\ k_{zr} &= \frac{1}{2}\sqrt{(2\omega s)^2 - \left|\vec{k}_r\right|^2} \approx k_{z0} + \left.\frac{dk_z}{ds}\right|_{s=so} (s_r - s_0). \end{aligned} \tag{39}$$

Equations (39) give the effective dispersion relation for which we need to implement the Jacobian weighting.

Appendix A outlines the derivation for the expresion of the Jacobian in variable velocity media. For the case of migration with output in offset, the Jacobian expression is:

$$\mathbf{W}_{k_h} = \left[\frac{\omega s_0}{k_{zs_0}} s_0 + \frac{\omega s_0}{k_{zs_0}} \left(2 - \left[\frac{\omega s_0}{k_{z0}} \right]^2 \right) (s_s - s_0) + \frac{\omega s_0}{k_{zr_0}} s_0 + \frac{\omega s_0}{k_{zr_0}} \left(2 - \left[\frac{\omega s_0}{k_{z0}} \right]^2 \right) (s_r - s_0) \right]^{-1} \tag{40}$$

where $(s_s - s_0)$ and $(s_r - s_0)$ are respectively the slowness perturbations at the source and receiver. In constant velocity media, $(s_s - s_0) = 0$ and $(s_r - s_0) = 0$, Equation (40) obviously takes the same form as Equation (23) we derived earlier for the case of constant velocity.

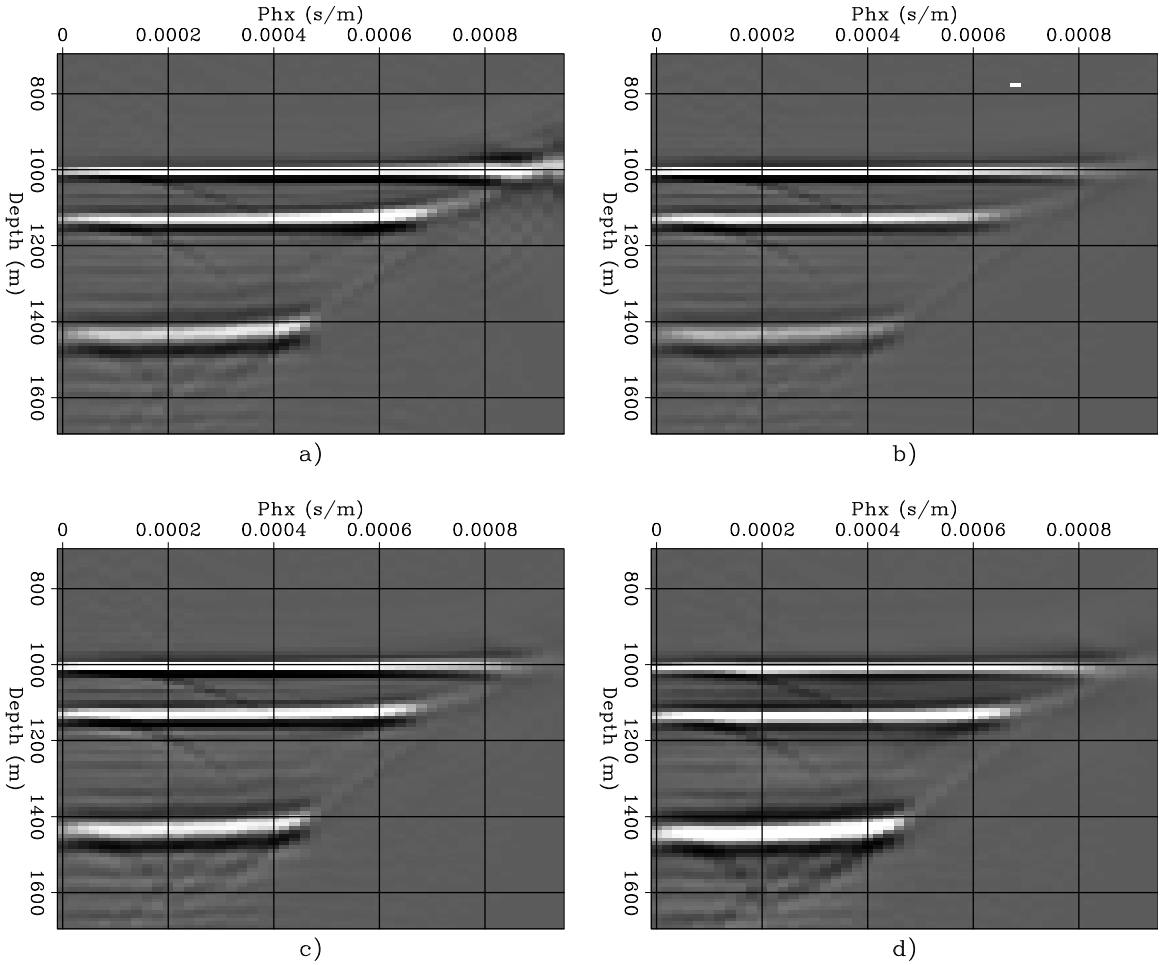

Figure 16: ADCIGs obtained by common-azimuth migration with different amplitude weights: a) No weights, b) $G^{-1}\mathbf{W}_{p_{hx}}^{\mathrm{CA}\ -1}$ (Jacobian), c) $G^{-1}A^{-1}\mathbf{W}_{p_{hx}}^{\mathrm{CA}\ -1}$ (Jacobian and WKBJ), d) $A_{\mathrm{stat}}^{-1}G^{-1}A^{-1}\mathbf{W}_{p_{hx}}^{\mathrm{CA}\ -1}$ (Jacobian, WKBJ, and stationary phase). The relative amplitudes of the dipping reflectors are modified by the different migration weights. paul2-CIG-amp [NR]

For the expressions of all Jacobians, we need to compute the quantity $\omega s/k_z$ which may lead to numerical instability when k_z approaches zero. A simple way so stabilize the Jacobian, which we have used for the current examples, is to add a small positive quantity to the denominator, and compute $\omega s/(k_z+\epsilon)$.

Another approach, which we have not tested yet, but which appears to have the potential to be more accurate, is to write

$$\begin{aligned}\frac{\omega s}{k_z} &= \frac{\omega s}{\frac{1}{2}\sqrt{(2\omega s)^2-\left|\vec{k}\right|^2}} \\ &= \frac{1}{\sqrt{1-\frac{\left|\vec{k}\right|^2}{[2\omega s]^2}}}.\end{aligned} \tag{41}$$

For *small values* of $x=\left|\vec{k}\right|/[2\omega s]$ we can compute $\omega s/k_z$ using the following Taylor series expansion:

$$\frac{1}{\sqrt{1-x^2}} \approx 1+\frac{1}{2}x^2+\frac{3}{8}x^4+\frac{5}{16}x^6+\frac{35}{128}x^8+\ldots \tag{42}$$

This expansion is very similar to the transformation used by Huang et al. (1999) for the extended Local Born Fourier migration method, or by Sava and Biondi (2000) in wave-equation MVA. This interesting possibility, however, awaits future research.

REAL DATA

We now provide, as an example, an image gather obtained for a real dataset. Figure 17 represents an offset ray-parameter gather at a particular horizontal location. According to the theory, in the absence of weighting, the amplitude at high p_h needs to be decreased, while the amplitude at low p_h needs to be increased.

The left panel shows the gather computed without the Jacobian weighting factor, while the right panel shows the gather after amplitude compensation. As expected, the Jacobian weighting attenuates most of the energy at high p_h, and enhances the amplitude of the reflections at lower p_h.

CONCLUSIONS

This paper demonstrates that angle-domain common image gathers generated by wave-equation migration can be used for AVA analysis if proper care is taken to ensure that amplitudes are not distorted during processing. Angle gathers can be computed both in the image space (with output in true reflection angle) or in the data space (with output in offset ray-parameter). The image-space method is independent of the structural dip. The two most important factors that

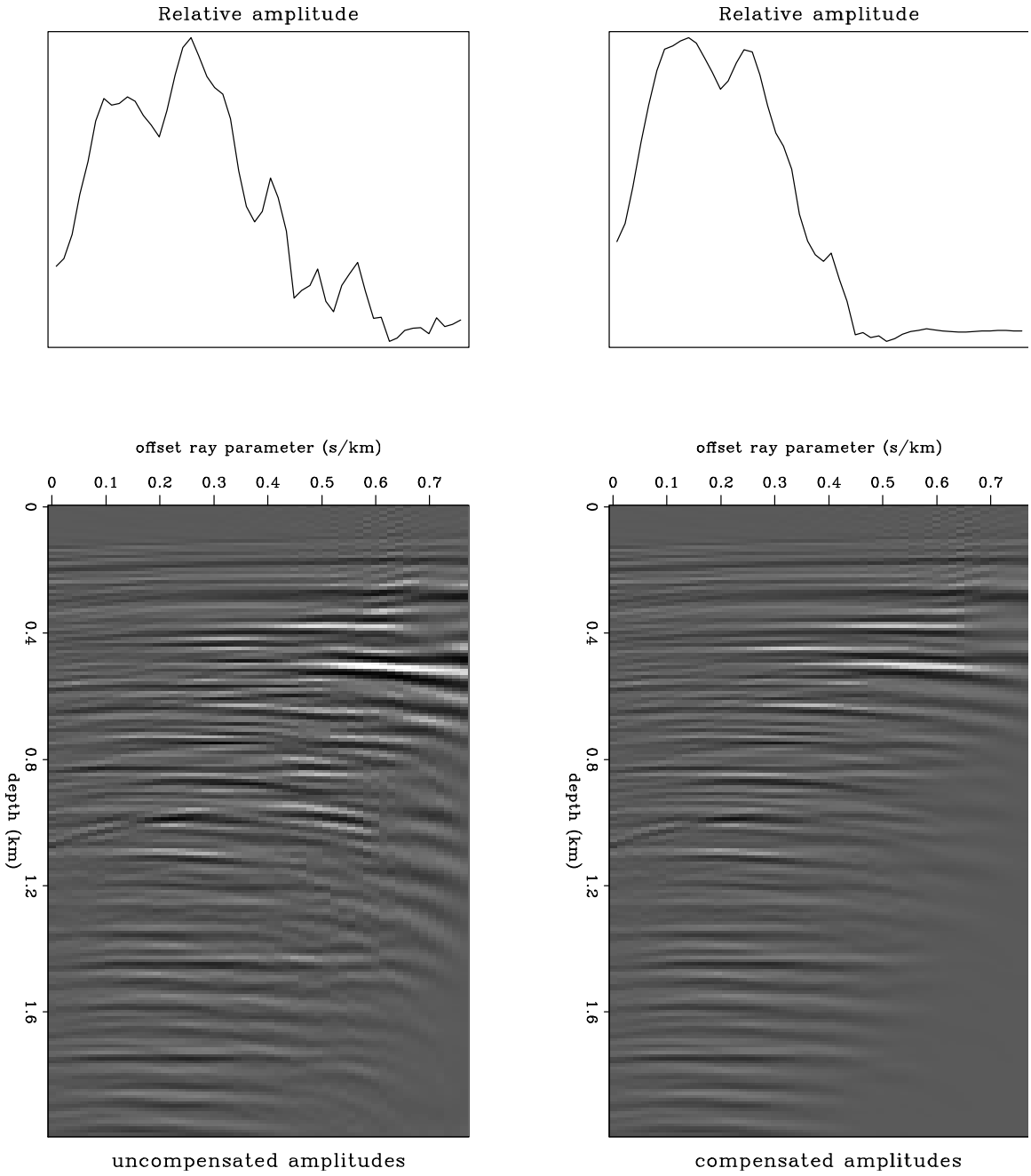

Figure 17: Real data example. The bottom panels are offset ray-parameter gathers computed with compensated (left) and uncompensated (right) amplitudes. The top panels show the amplitude variation with offset ray parameter for an event at about 1.75 km depth. The amplitude decrease at small incidence angles is caused by the absence of innermost offsets from the recorded data. paul2-kja10.5 [NR]

influence the accuracy of the amplitude response are the sampling of the offset axis and the incorrect treatment of amplitudes during migration. While the limited sampling cannot be corrected, the migration operator can be modified to incorporate the appropriate correction factors. We have analyzed the Jacobian compensation factors, and show that they can successfully be applied to real data. We have shown how to construct "true amplitude" wave-equation migration operators, as well as pseudo-unitary modeling and migration operators.

ACKNOWLEDGMENTS

This research was partially funded by the ACTI project #4731$U0015-3Q$. Some of this work was prompted by discussions with John Etgen at BP.

REFERENCES

Biondi, B., and Palacharla, G., 1996, 3-D prestack migration of common-azimuth data: Geophysics, **61**, no. 6, 1822–1832.

Biondi, B. L., 1999, 3-D Seismic Imaging: `http://sepwww.stanford.edu/sep/biondo/Lectures/index.html`.

Biondi, B., 2001, Narrow-azimuth migration: Analysis and tests in vertically layered media: SEP–**108**, 105–118.

Bleistein, N., and Handelsman, R. A., 1975, Asymptotic expansions of integrals: Rinehart Winston.

Claerbout, J. F., 1995, Basic Earth Imaging: Stanford Exploration Project.

Clayton, R. W., and Stolt, R. H., 1981, A Born-WKBJ inversion method for acoustic reflection data: Geophysics, **46**, no. 11, 1559–1567.

de Bruin, C. G. M., Wapenaar, C. P. A., and Berkhout, A. J., 1990, Angle-dependent reflectivity by means of prestack migration: Geophysics, **55**, no. 9, 1223–1234.

Fomel, S., 1996, Migration and velocity analysis by velocity continuation: SEP–**92**, 159–188.

Huang, L., Fehler, M. C., and Wu, R. S., 1999, Extended local Born Fourier migration method: Geophysics, **64**, no. 5, 1524–1534.

Ottolini, R., 1982, Migration of reflection seismic data in angle-midpoint coordinates: Ph.D. thesis, Stanford University.

Prucha, M., Biondi, B., and Symes, W., 1999, Angle-domain common-image gathers by wave-equation migration: 69th Ann. Internat. Meeting, Soc. Expl. Geophys., Expanded Abstracts, 824–827.

Prucha, M. L., Clapp, R. G., and Biondi, B. L., 2001, Imaging under salt edges: A regularized least-squares inversion scheme: SEP–**108**, 91–104.

Rickett, J., 2001, Model-space vs data-space normalization for finite-frequency depth migration: SEP–**108**, 81–90.

Sava, P., and Biondi, B., 2000, Wave-equation migration velocity analysis: Episode II: SEP–**103**, 19–47.

Sava, P., and Fomel, S., 2000, Angle-gathers by Fourier Transform: SEP–**103**, 119–130.

Stolt, R. H., and Benson, A., 1986, Seismic migration — theory and practice: Geophysical Press, London - Amsterdam.

Stolt, R. H., 1978, Migration by Fourier transform: Geophysics, **43**, no. 1, 23–48.

Wapenaar, K., Van Wijngaarden, A., van Geloven, W., and van der Leij, T., 1999, Apparent AVA effects of fine layering: Geophysics, **64**, no. 6, 1939–1948.

APPENDIX A

This appendix presents a derivation of the expression for the weighting Jacobian in the case of variable velocity.

The dispersion relation

$$k_z = \frac{1}{2}\sqrt{(2\omega s)^2 - |k|^2} \tag{A-1}$$

can be approximated using a Taylor series expansion around the constant reference slowness (s_0):

$$k_z \approx k_{z0} + \left.\frac{dk_z}{ds}\right|_{s=so} (s - s_0). \tag{A-2}$$

We then take the derivative of k_z with respect to the frequency ω

$$\frac{dk_z}{d\omega} = \frac{dk_{z0}}{d\omega} + \frac{d}{d\omega}\left[\frac{dk_{z0}}{ds}\right](s - s_0),$$

and if we note that

$$\frac{dk_{z0}}{ds} = \frac{\omega^2 s_0}{k_{z0}}$$

we obtain

$$\frac{dk_z}{d\omega} = \frac{dk_{z0}}{d\omega} + \frac{d}{d\omega}\left[\frac{\omega^2 s_0}{k_{z0}}\right](s - s_0). \tag{A-3}$$

We continue by evaluating the derivatives with respect to ω on the right hand side. With little algebra, we obtain

$$\frac{d}{d\omega}\left[\frac{\omega^2 s_0}{k_{z0}}\right] = \frac{\omega s_0}{k_{z0}}\left(2 - \left[\frac{\omega s_0}{k_{z0}}\right]^2\right).$$

therefore

$$\frac{dk_z}{d\omega} = \frac{\omega s_0}{k_{z0}} s_0 + \frac{\omega s_0}{k_{z0}}\left(2 - \left[\frac{\omega s_0}{k_{z0}}\right]^2\right)(s - s_0). \tag{A-4}$$

The prestack weighting Jacobian is:

$$\mathbf{W}_{k_h} = \left[\frac{\omega s_0}{k_{zs_0}} s_0 + \frac{\omega s_0}{k_{zs_0}}\left(2 - \left[\frac{\omega s_0}{k_{z0}}\right]^2\right)(s_s - s_0) + \frac{\omega s_0}{k_{zr_0}} s_0 + \frac{\omega s_0}{k_{zr_0}}\left(2 - \left[\frac{\omega s_0}{k_{z0}}\right]^2\right)(s_r - s_0)\right]^{-1} \tag{A-5}$$

which, in constant slowness, takes the simple form

$$\mathbf{W}_{k_h} = \left[\frac{\omega s_0}{k_{zs_0}} s_0 + \frac{\omega s_0}{k_{zr_0}} s_0\right]^{-1}. \tag{A-6}$$